Chemical Science

ROYAL SOCIETY
OF **CHEMISTRY**

EDGE ARTICLE
D. E. De Vos *et al.*
Evolution of the active species of homogeneous Ru
hydrodeoxygenation catalysts in ionic liquids

Evolution of the active species of homogeneous Ru hydrodeoxygenation catalysts in ionic liquids†

K. Janssens, [a] A. L. Bugaev, [bc] E. G. Kozyr, [bd] V. Lemmens,[a] A. A. Guda,[b] O. A. Usoltsev, [b] S. Smolders, [a] A. V. Soldatov[b] and D. E. De Vos [*a]

This work establishes structure–property relationships in Ru-based catalytic systems for selective hydrodeoxygenation of ketones to alkenes by combining extensive catalytic testing, *in situ* X-ray absorption spectroscopy (XAS) under high pressures and temperatures and *ex situ* XAS structural characterization supported by density functional theory (DFT) calculations. Catalytic tests revealed the difference in hydrogenation selectivity for ketones (exemplified by acetone) or alkenes (exemplified by propene) upon changing the reaction conditions, more specifically in the presence of CO during a pretreatment step. XAS data demonstrated the evolution of the local ruthenium structure with different amounts of Cl/Br and CO ligands. In addition, in the absence of CO, the catalyst was reduced to Ru⁰, and this was associated with a significant decrease of the selectivity for ketone hydrogenation. For the Ru−bromide carbonyl complex, selectivity towards acetone hydrogenation over propene hydrogenation was explained on the basis of different relative energies of the first intermediate states of each reaction. These results give a complete understanding of the evolution of the Ru species, used for the catalytic valorization of biobased polyols to olefins in ionic liquids, identifying the undesired deactivation routes as well as possibilities for reactivation.

Introduction

The selection of ligands in the coordination sphere of homogeneous catalysts allows for the tuning of process-specific, chemoselective hydrogenations.[1] As a prominent example, the chemoselectivity of $RuCl_2(PPh_3)_2$ can be shifted from olefin hydrogenation[2] to carbonyl hydrogenation,[3] as discovered by Noyori and coworkers. This was achieved through the addition of a vicinal diamine, *e.g.* ethylenediamine, and a base, *e.g.* KOH, revealing a new way to catalytically hydrogenate the carbonyl group.[4] For the preferential hydrogenation of carbonyl groups in the presence of C═C functions, this approach allows replacement of stochiometric metal hydride reagents, such as $NaBH_4$ or $LiAlH_4$, by molecular hydrogen and a catalyst.

Other homogeneous Ru-complexes are also known to be active catalysts for hydrogenation of aldehydes and ketones, but

aCentre for Membrane Separations, Adsorption, Catalysis and Spectroscopy for Sustainable Solutions (cMACS), KU Leuven, Celestijnenlaan 200F, Post Box 2454, 3001 Leuven, Belgium. E-mail: dirk.devos@kuleuven.be

bThe Smart Materials Research Institute, Southern Federal University, Sladkova 178/ 24, 344090 Rostov-on-Don, Russia. E-mail: abugaev@sfedu.ru

cSouthern Scientific Centre, Russian Academy of Sciences, Chekhova 41, 344006 Rostov-on-Don, Russia

dDepartment of Chemistry, University of Turin, Via Giuria 5, 10125 Torino, Italy

† Electronic supplementary information (ESI) available: Details of Product analysis, catalytic tests, XAS analysis and DFT calculations. See https://doi.org/10.1039/d2sc02150a

whether they also refrain from reacting with C═C bonds, is not always clear. Braca *et al.* reported that Ru halide carbonyls, even without PPh₃, catalyze the hydrogenative dehydroxylation of glycerol and sugar alcohols, which proceeds in acidic conditions.[5] For instance, in the presence of $[Ru(CO)_3I_2]_2$ as a homogeneous catalyst, and of hydrogen iodide as a Brønsted acid, glycerol is converted to *n*-propanol. After the Brønsted acidity dehydrates glycerol to acrolein, the Ru catalyst performs a complete hydrogenation of both the olefin and aldehyde functions, yielding 1-propanol and the derived ether. Clearly, under these acidic dehydration conditions, the Ru catalysts do not discriminate between C═C and C═O bonds. In contrast, our group has developed an alternative approach to the hydrodeoxygenation of sugar alcohols and glycerol to olefins. When HBr/Bu_4PBr as a Brønsted acidic ionic liquid (IL) is combined with a Ru halide carbonyl hydrogenation catalyst, mono-alkenes are obtained selectively from sugar alcohols.[6,7] In contrast to previous work, the dehydration in this process relies on acid-promoted Br⁻ substitution–elimination reactions; the hydrogenation is performed by *in situ* formed $RuBr_x(CO)_y$ compounds. These were observed to be generated *in situ* from RuBr₃ and CO, formed by decarbonylation of the formed aldehyde intermediates, or by the thermal decomposition of formaldehyde.[6] Later, an additional pretreatment step involving CO gas proved useful to obtain even higher selectivities in the valorization of crude waste glycerol to propylene.[7] Remarkably, the product alkenes are hardly hydrogenated. However, apart

from the proof that CO drastically improves the biomass valorization in terms of olefin selectivity, no clear understanding of the catalytic system is available.

Here, we elucidate the different catalytic steps in the Ru-catalyzed hydrodeoxygenation of glycerol to propene by monitoring the evolution of Ru-species by *in situ* X-ray absorption spectroscopy (XAS) and performing additional detailed analysis of the high-quality *ex situ* data collected by carefully trapping different intermediate states in solidified ionic liquid. The different states are correlated to the separate activation and deactivation steps. First, we focus on the catalyst dissolution in the IL, to reveal whether the Ru precursors remain stable or are converted into new complexes. Then, we investigate the impact of CO gas, to correlate the actual ligand environment of Ru to the catalytic performance. Finally, the origin of the selectivity towards ketone hydrogenation is supported with theoretical density functional theory (DFT) calculations.

Materials and methods

Catalytic reaction

A typical reaction mixture consists of a homogeneous Ru catalyst (10 µmol) dissolved in Bu_4PBr (1.7 mmol, 577 mg), acetone (0.50 mmol, 37.0 µL) or propene (1 bar) as the model reactants, H_2 gas as the reducing agent, in the presence of a mixture of dodecane (1 mL, extraction solvent) and tetradecane (0.5 mmol, 0.13 mL, internal standard). First, all solids and liquids are loaded into a glass liner (5 ml) inside a stainless steel pressure reactor. Next, the reactor is flushed 3 times with N_2 followed by H_2, loaded optionally with propene gas (1 bar) and finally with 40 bar of H_2. Occasionally, prior to the actual catalytic reaction, an additional pretreatment step was performed to generate Ru bromide carbonyl species through stirring of $RuBr_3$ in the IL under 1 bar of CO gas and 40 bar of H_2 for 30 minutes at 180 °C. Catalytic reactions were performed by stirring the total reaction mixture for 1 h at 220 °C.

After reaction, the reactor was cooled on ice and a gaseous sample was taken for FTIR gas phase analysis. The yield of apolar compounds was determined *via* GC analysis of the dodecane layer. Finally, a derivatisation reaction was performed on the polar IL layer using *N,O*-bis(trimethylsilyl)-trifluoroacetamide (BSTFA, 400 µL), silylating the alcohols remaining in that layer. All products were analyzed according to previous literature procedures.[6,7] Details on the product analysis and the boundary conditions for the catalytic reaction are provided in the ESI.†

Synthesis of [RuBr_2(CO)_3]_2

The Ru bromide carbonyl complex was synthesized according to a literature procedure.[7,8] $Ru_3(CO)_{12}$ (0.129 g, 0.20 mmol) was dissolved in dry benzene resulting in an orange solution. Excess Br_2 was added and the solution was stirred vigorously for 3 hours. The solvent and unreacted Br_2 were removed under reduced pressure. The crude product was purified by recrystallization in chloroform/hexane resulting in a yellow solid. The identity of the $[RuBr_2(CO)_3]_2$ complex was confirmed with FT-IR

spectroscopy and Electrospray Ionization Mass Spectrometry (ESI-MS). FTIR analysis was performed in a Bruker IFS 66v/S FTIR spectrometer under vacuum. The ESI-MS was conducted in positive ion mode with a Thermo Finnigan LCQ Advantage mass spectrometer. $\nu(CO)$: (KBr) 2138 cm^{-1} (s), 2078 (s) cm^{-1}, ESI-MS (MH^+ in CH_3CN): 387.75; found, 388.0. XAS analysis (Fig. S7†) also provided the 3D atomic structure of the complex.[9,10]

Ex situ XAS data collection

Experimental Ru *K*-edge XAS data were measured at the BM23 beamline of ESRF (Grenoble, France) and CLAESS beamline of ALBA (Barcelona, Spain). The powdered reference samples were pressed into pellets to optimize the absorption jump at the Ru *K*-edge. The catalytic samples frozen in the IL were placed in a self-made teflon container of cylindrical shape, closed from both sides with Kapton tape. To exclude the effect of dilution in the IL, the reference complexes were measured both pure in the crystalline state and diluted in Bu_4PBr at high or low concentrations. For the diluted reference samples, both powders were heated 10 °C above the IL melting point ($T_{melting} = 100$ °C) and stirred vigorously. High concentrations (Ru : Br ratio of *ca.* 1 : 35) resulted in good signal-to-noise ratio in both X-ray absorption near edge structure (XANES) and extended X-ray absorption fine structure (EXAFS) regions. However, in standard catalytic reactions the system is ~5 times more diluted, resulting in an Ru : Br ratio of 1 : 170. The presence of the strongly absorbing Br limits signal intensity in the lower edge jump compared to reference samples and, therefore, more noisy data are obtained in the EXAFS region. All spectra were collected in the transmission mode, which showed better signal-to-noise ratio compared to the fluorescence signal collected in similar acquisition times, with simultaneous measurement of metallic ruthenium foil for energy alignment. The filling of the 1st, 2nd and 3rd ionization chambers resulted in the absorption of 20, 80, and 80%, respectively, at the Ru *K*-edge photon energy. The energy was selected by a Si(311) double-crystal monochromator operated in a step mode. Rejection of higher harmonics was done by Rh coated mirrors. The energy steps in the pre-edge and XANES regions were 5 and 1 eV respectively. In the EXAFS region, a constant step in *k*-space of 0.035 $Å^{-1}$ was used. At B22, continuous scanning mode was used.

In situ XAS data collection

In situ Ru *K*-edge XAS spectra were collected in fluorescence mode at the SAMBA beamline of Soleil synchrotron (Paris, France). A sample containing similar concentrations of reagents, as used for the catalytic tests, was loaded into a self-made high-pressure reactor (Fig. S1†) which had the same geometry as the reactors used for the catalytic tests. The cell was pressurized with H_2 and CO and heated by four built-in thermistor elements. The magnetic stirrer was positioned below the cell (Fig. S1b†). The energy was scanned continuously by a Si(220) monochromator. The I_0 intensity before the sample was collected by an ionization chamber and the fluorescence signal was collected by a Vortex silicon drift detector. The energy

was calibrated with a ruthenium foil before each *in situ* run; this did not demonstrate significant drifts of the monochromator.

XAS data analysis

Initial processing of experimental XAS data, including normalization, energy calibration, extraction of $\chi(k)$ signals and further Fourier analysis of EXAFS, were performed in the Athena and Artemis programs of the Demeter package.[11] The fitting was done in R-space in the 1–3 Å range simultaneously on k^1-, k^2-and k^3-weighted data, Fourier-transformed applying the Hanning window from 4 to 15 $Å^{-1}$ with $dk = 1$. For the reference compounds the signals up to $k = 18$ $Å^{-1}$ were also examined. The theoretical phases and amplitudes were calculated by FEFF6.[12] The *in situ* XAS data were processed in the Fastosh program. Principle component analysis (PCA) analysis was performed in PyFitIt code.[13] Multivariate curve resolution alternating least squares (MCR-ALS) analysis of the *in situ* data (in the XANES region) was performed by means of the MATLAB code.[14–16]

DFT calculations

Geometry relaxation and calculation of reaction enthalpies were done in ADF software[17] at DFT level of theory with BLYP-D3 exchange-correlation potential[18–20] and TZP Slater-type basis set.[21] The choice of the potential and basis set was made based on the comparison of the Ru–ligand C, Ru–Cl and C–O distances in the relaxed structure with those obtained from EXAFS for $[RuCl_2(CO)_3]_2$. The scalar relativistic effects were included within the Zero Order Regular Approximated (ZORA) Hamiltonian.[22]

Results and discussion

Catalytic testing

Previous reports on the use of HBr/Bu_4PBr as the dehydrating solvent for the valorisation of biobased vicinal alcohols suggested a pathway relying on substitution with Br^- and HBr elimination, rather than an E_1 mechanism. This results in a specific dehydration route mainly leading through ketone, rather than aldehyde intermediates.[6] In the reaction of erythritol, butanone hydrogenation was found to be a kinetically slow step, whereas the hydrogenation of 2,3-butanedione and α-hydroxycarbonyl compounds occurs faster, possibly due to the directing role of the second oxygen functionality.[6] Similar results were obtained in the case of glycerol, where acetone was detected as the carbonyl intermediate that is slowest to be converted.[7] In absence of the HBr acid co-catalyst, over 50% of unconverted alcohol products (mainly 1,2-PDO and glycerol) were reported, indicating the importance of HBr to fully convert biobased polyol intermediates to the desired olefins.[6,7] Most decisive for the olefin selectivity is the ability to hydrogenate ketones like butanone or acetone, while leaving the desired propene or butene products intact. In order to elucidate the role of the various Ru species in either ketone or olefin hydrogenation, acetone and propene were used as model reactants (Scheme 1). Several ruthenium catalysts (commercial $RuBr_3$ and

$[RuCl_2(CO)_3]_2$, and synthesized $[RuBr_2(CO)_3]_2$) were tested on either substrate under realistic conditions, similar to those of the conversion of (waste) glycerol to propene (Table 1). Ru bromide carbonyl compounds were obtained in two different ways: *via* a classical, *ex situ* way, as reported by Johnson *et al.*, starting from $Ru_3(CO)_{12}$ and Br_2 leading to $[RuBr_2(CO)_3]_2$ (entries 3 and 10 in Table 1),[8,23] and by an *in situ* exposure of $RuBr_3$ dissolved in the IL to CO gas in a pretreatment step (entries 4–6, 11–13).[7] For the hydrogenation of acetone with different Ru precursors, key observations are summarized in Table 1 (entries 1–7). The presence of CO in the catalyst coordination sphere seems strictly necessary to obtain an active catalyst for ketone hydrogenation, with $RuBr_3$ (entry 1) only resulting in non-selective conversion of acetone (presumably *via* condensation reactions).[6] Remarkably, depending on the catalyst synthesis, a distinct product distribution is observed (entries 2–3 *vs.* 4–5). In the case of the pre-isolated $[RuX_2(CO)_3]_2$ complexes, less dehydration reactions are occurring (up to 30% alcohols remaining), with significant overhydrogenation to the undesired alkanes (less than 40% olefin selectivity). A pretreatment step with CO gas on the *ex situ* synthesized $[RuBr_2(CO)_3]_2$ improved the propene selectivity significantly, but further decreased the dehydration activity (entry 4). In contrast, a similar complex formed *in situ* starting from Ru(III) $Br_3 \cdot xH_2O$ results in near quantitative dehydration, maintaining very high olefin selectivity (entry 5). Even after extending the reaction time to 4 hours there is only a minor increase in olefin overhydrogenation to propane (entry 6). The increase in alcohol conversion might be due to *in situ* formation of HBr, as a result of reduction of Ru(III)Br_3 to $[Ru(II)Br_2(CO)_x]_2$. This results in an increase in Brønsted acidity and free Br^- in the system, while the additional CO ligands allow for more catalyst stability and selectivity in the two competitive hydrogenation steps.

Next, it was evaluated whether the choice of the Ru precursor has an effect on the preservation of propene, thus on avoiding overhydrogenation to the undesired alkane (entries 8–14). $RuBr_3$ shows the highest overhydrogenation in the absence of a CO pretreatment step (entry 8). The overhydrogenation decreases for the isolated complexes (entries 9 and 10), also upon addition of a CO pretreatment step (entry 11). Finally, it is found to be almost negligible for the *in situ* formed complex (entry 12) as the increased acidity may additionally prevent the reduction to zerovalent Ru metal. Extending the reaction time to 4 h (entry 13) shows only a minor formation of propane from propene, indicating that high catalyst stability is combined with impressive C=O *vs.* C=C selectivity. The necessity of a pretreatment step under CO, rather than applying CO directly during the reaction, was confirmed by a control experiment on
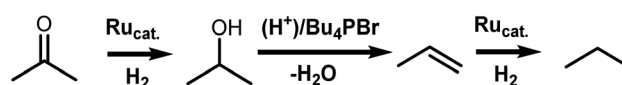
Scheme 1 Simplified system to study the two key hydrogenation steps in the valorization of biobased alcohols with catalytic Ru and IL: (1) reduction of ketone intermediates to alcohols; (2) avoiding overhydrogenation of the desired olefin end products.

Table 1 Hydrogenation of acetone and fate of propene in the presence of different homogeneous Ru catalysts[a]

Entry	Catalyst	Substrate[e]	Olefin Selectivity[f]	Propene[g] (%)	Propane[g] (%)	Isopropanol[h] (%)	Acetone[g] (%)
0	$RuBr_3 \cdot xH_2O + CO^b$	Glycerol	94%	82	5	2	4
1	$RuBr_3 \cdot xH_2O$	Acetone	/[i]	2	<1	<1	53
2	$[RuCl_2(CO)_3]_2$	Acetone	36%	25	44	26	3
3	$[RuBr_2(CO)_3]_2$	Acetone	30%	17	40	29	8
4	$[RuBr_2(CO)_3]_2 + CO^b$	Acetone	52%	25	23	46	4
5	**$RuBr_3 \cdot xH_2O + CO^b$**	**Acetone**	**90%**	**77**	**8**	**2**	**<1**
6	$RuBr_3 \cdot xH_2O + CO^{b,c}$	Acetone	82%	72	16	<1	<1
7	$RuBr_3 \cdot xH_2O + CO^{b,d}$	Acetone	93%	40	3	1	50
8	$RuBr_3 \cdot xH_2O$	Propene	39%	38	59	—	—
9	$[RuCl_2(CO)_3]_2$	Propene	56%	52	41	—	—
10	$[RuBr_2(CO)_3]_2$	Propene	63%	62	36	—	—
11	$[RuBr_2(CO)_3]_2 + CO^b$	Propene	82%	78	17	—	—
12	**$RuBr_3 \cdot xH_2O + CO^b$**	**Propene**	**96%**	**95**	**4**	—	—
13	$RuBr_3 \cdot xH_2O + CO^{b,c}$	Propene	87%	84	13	—	—
14	$RuBr_3 \cdot xH_2O + CO^{b,d}$	Propene	98%	93	2	—	—

[a] Reaction conditions unless stated otherwise: 0.01 mmol $Ru_{cat.}$ (2 mol%), 1.7 mmol Bu_4PBr, 1 mL dodecane, 0.5 mmol tetradecane (IS), 220 °C, 40 bar H_2, 1 h. [b] Pretreatment step of $RuBr_3$ with CO gas (1 bar), 30 min, 40 bar H_2, 180 °C. [c] Reaction for 4 h. [d] CO gas (1 bar) present during the reaction. [e] Glycerol: ref. 7: HBr co-catalyst (5 mol%), crude glycerol (0.5 mmol). Acetone (0.5 mmol, 36.7 μL). Propene gas (1 bar). [f] Ratio of propene *vs.* (propene + propane) determined by FT-IR/GC gas analysis. [g] GC yield. [h] GC yield after BSTFA derivatization. [i] Yield too low to allow reliable selectivity determination.

both acetone and propene (entries 7 and 14). We have previously obtained similar results in the HDO of erythritol, with butanone as the model substrate.[6] Indeed, when the reaction is performed under 1 bar of CO, not only the olefin is hardly hydrogenated (entry 14); also the carbonyl hydrogenation is significantly hampered, presumably due to oversaturation of the catalyst coordination sphere with CO. Besides catalyst stability and selectivity, also catalyst recyclability is an important criterion. Therefore, after CO pretreatment, the catalyst was reused in 5 runs, showing clear selectivity loss if no CO is added in between cycles (Fig. 1). Selectivity is perfectly preserved when CO is added in between cycles.

Ru speciation in IL upon dissolution

In the following, the solidification of the IL at room temperature ($T_{melting} = 100$ °C) is used as a unique feature to trap the catalytic species, in order to clarify the behavior of the different Ru compounds by XAS (*vide supra*; *ex situ* XAS data collection). Spectra recorded for RuX_3 (X = Br, Cl) salts admixed in Bu_4PBr,
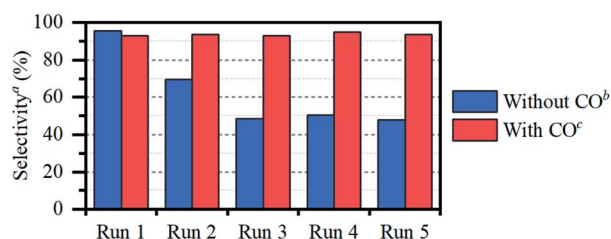
show that higher-shell FT-EXAFS peaks are eliminated (Fig. 2b); this confirms their dissolution. At the same time, there is no shift in the edge position of the XANES spectra (Fig. 2a), indicating that the oxidation state of Ru is not changed. The results of Fourier-analysis of EXAFS data are reported in Table S1.† For $RuBr_3$ in the ionic liquid, the first-shell coordination number
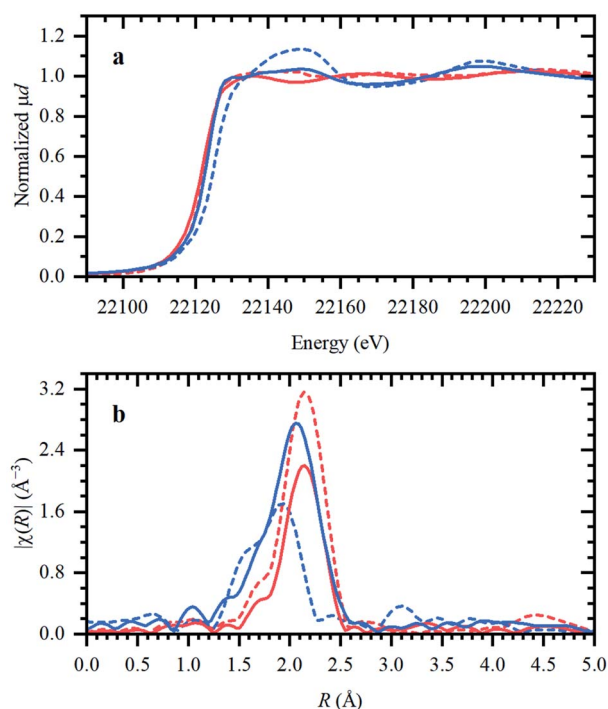

Fig. 1 Preservation of propene over multiple runs. [a]Fraction of propene in the (propene + propane) fraction. Conditions: $RuBr_3 \cdot xH_2O$ (2 mol%), propene (1 bar), Bu_4PBr (577 mg, 3.4 mmol). Pretreatment: CO gas (1 bar) 40 bar H_2, 0.5 h, 180 °C. Each hydrogenation uses a fresh charge of propene gas (1 bar), 40 bar H_2, 1 h, 220 °C. [b]CO pretreatment before first run. [c]CO pretreatment before each run.

Fig. 2 XANES (a) and magnitudes of Fourier-transformed (4–15 Å^{-1}) phase-uncorrected FT-EXAFS (b) data for $RuBr_3$ (red) and $RuCl_3$ (blue), before (dashed lines) and after (solid lines) dissolution in Bu_4PBr.

(CN) decreases from 6 to 4.3 ± 0.3. This could be explained by 4-coordinated $[RuBr_4]^-$ complexes with additional Br^- coming from the IL. For $RuCl_3$, a significant reshaping of both EXAFS and XANES data is observed, associated with a Cl^-–Br^- exchange in Br-rich IL. The resulting structure contains a mixture of $RuCl_x$ and $RuBr_y$ species, with clearly visible Ru–Cl and Ru–Br contributions in FT-EXAFS. To overcome the instabilities, the total CN was fixed to 4.

Next, isolated $[RuX_2(CO)_3]_2$ precursors were used instead of RuX_3 compounds (X = Br, Cl). The corresponding XANES and EXAFS data are shown in Fig. 3. As in the previous case, the strongest changes in the spectra are observed for the Cl-containing precursor, which is also associated with Cl^-–Br^- exchange. This is supported by DFT calculations since the reaction of 4 Bu_4PBr + $[RuCl_2(CO)_3]_2$ to form $4Bu_4PCl$ + $[RuBr_2(CO)_3]_2$ is favourable with ΔH of about (−3)–(−4) kcal mol^{-1} (Fig. S5†). In addition, after dissolution in IL, both precursors exhibit increased Ru–Br and decreased Ru–CO contributions in EXAFS (Fig. 3b). The Ru–Br coordination is increased roughly by 1 (see Table S2†) with respect to the reference $[RuBr_2(CO)_3]_2$ complex. This can be explained by a loss of CO ligands to the gas phase.

Two aspects related to the Ru speciation upon dissolution in the IL are noteworthy. First, irrespective of the original precursor, a complex with Br-ligands is formed in Bu_4PBr due to Cl^-–Br^- exchange. Secondly, the IL itself is not sufficient to preserve the structure of the isolated $[RuX_2(CO)_3]_2$ complexes upon dissolution, explaining their significantly lower catalytic performance (Table 1; entry 2–3 and 9–10). Since the structure of the isolated Ru-precursors is not preserved ($CN_{CO} < 3$), it might only be possible to form the actual catalytic complex in the IL through the CO pretreatment step.

The role of CO and reaction conditions

The presence of CO gas (during the pretreatment) transforms the $RuBr_3$ salt (Fig. 4, dashed black vs. gray spectra for $RuBr_3$ before & after dissolution in the IL) into Ru carbonyl species (solid blue), with a spectrum highly similar to that of the crystalline $[RuBr_2(CO)_3]_2$ reference compound (dashed red). This shift in the Ru speciation (from dashed grey to solid blue) is reflected in the very high selectivity for carbonyl vs. olefin hydrogenation (entries 5, 12). The structure was also compared with the one formed in presence of formaldehyde as a CO source, according to the procedure reported in our previous work.[6] The latter also results in a similar ruthenium halide carbonyl complex, but with increased Ru–Br and decreased Ru–CO contributions compared to the sample obtained under CO gas (Fig. S2†). This again can be assigned to a partial decomposition of the priorly isolated $[RuBr_2(CO)_3]_2$ into Ru bromide carbonyl species ($CN_{CO} < 3$), explaining the significant decrease in olefin selectivity shown for glycerol.[7] The low concentration of Ru in the systems tested under CO pretreatment and under reaction conditions complicates EXAFS analysis, but XANES spectra give a clear indication of the relative changes in the number of CO and Br ligands over the whole series of samples.
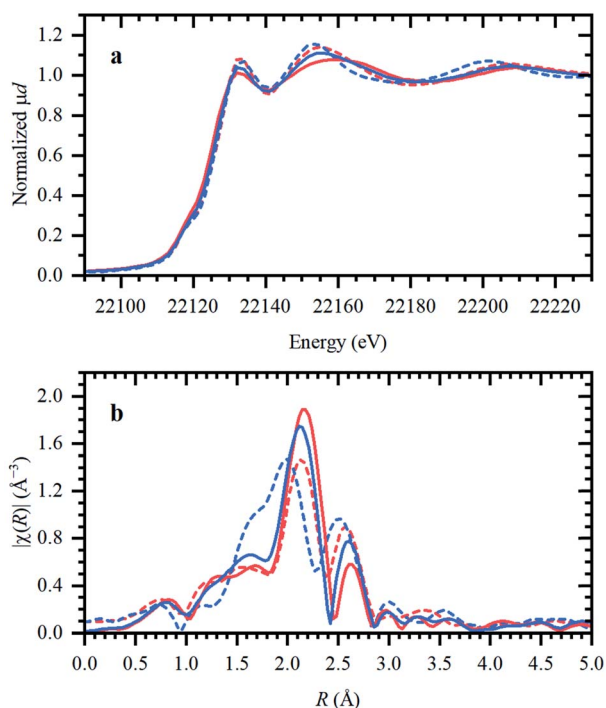

Fig. 3 XANES (a) and magnitudes of Fourier-transformed (4–15 Å^{-1}) phase-uncorrected FT-EXAFS (b) data for $[RuBr_2(CO)_3]_2$ (red) and $[RuCl_2(CO)_3]_2$ (blue), before (dashed lines) and after (solid lines) dissolution in Bu_4PBr.
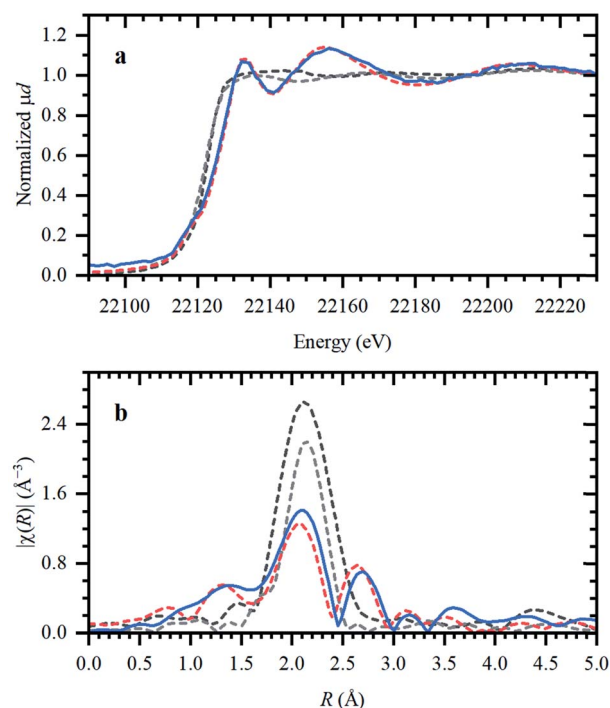

Fig. 4 XANES (a) and phase-uncorrected FT-EXAFS (b) data for the reference $RuBr_3$ salt (dashed black) and $[RuBr_2(CO)_3]_2$ compound (dashed red), and $RuBr_3$ salt dissolved in Bu_4PBr without (dashed grey) and with (solid blue) addition of CO gas.

A linear combination fitting (LCF) using two reference spectra of $RuBr_3$ and $Ru_3(CO)_{12}$ was performed to reveal the relative ratio of these components in the studied samples (Fig. 5). For RuX_3 dissolved in IL, the fraction of $RuBr_3$ component is close to 1, but in the presence of CO during the pretreatment step, this sample almost fully (*ca.* 92%) converts to $[RuBr_2(CO)_3]_2$ (reference) species. After reaction or upon dissolution of the pre-isolated reference in IL the $[RuBr_2(CO)_3]_2$-complex partially degrades to $RuBr_x$ species, which can be associated with deactivation of the catalysts in absence of CO (*vide supra*). This can be counteracted by CO pretreatment in between the cycles (Fig. 1). Finally, if $RuBr_3$ is used in absence of CO, formation of small Ru^0 clusters occurs after reaction due to the presence of the reducing H_2 gas (Fig. 6). These species are
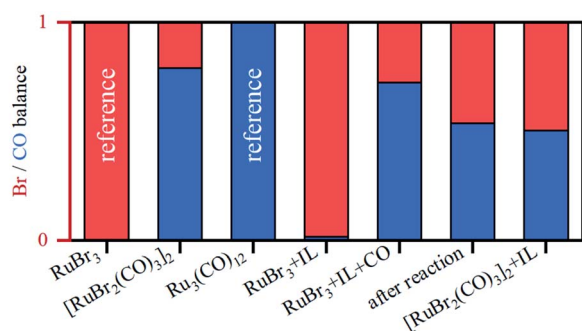
Fig. 5 Relative fractions of Br (shown in red) *vs.* CO (in blue) in the Ru coordination sphere, for different samples, as obtained by LCF analysis.
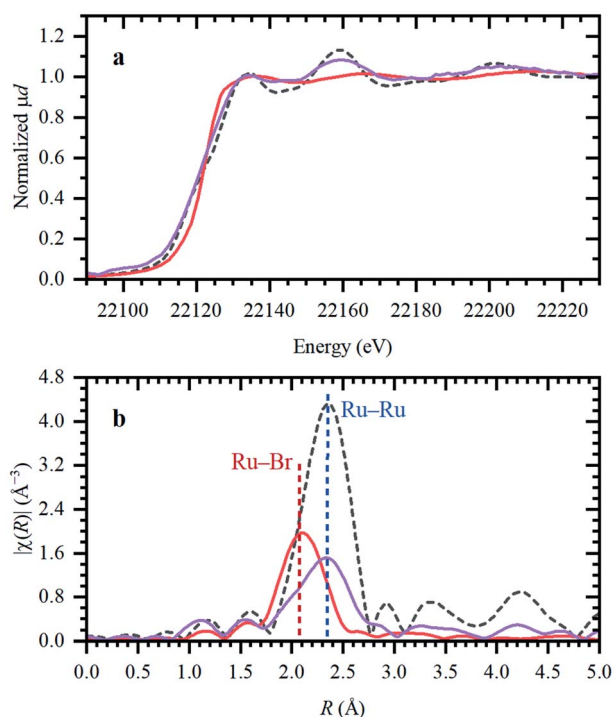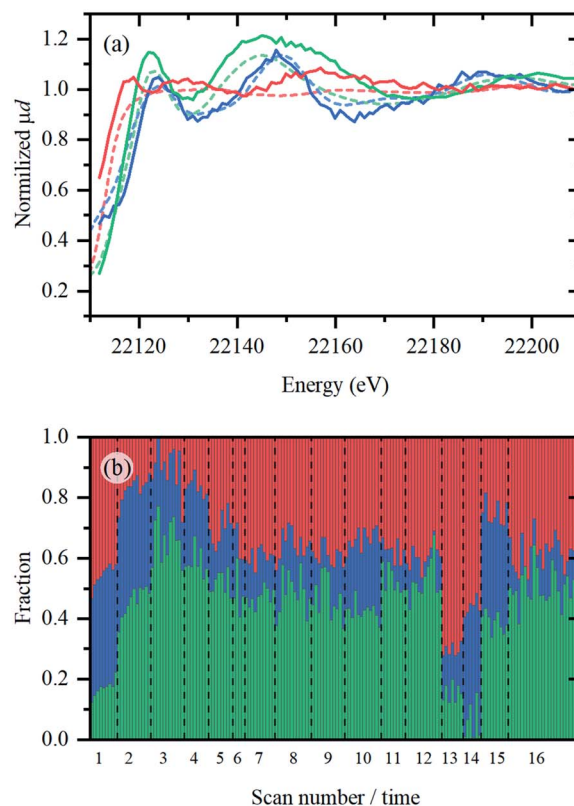

Fig. 6 XANES (a) and phase-uncorrected FT-EXAFS (b) data for $RuBr_3$ salt dissolved in IL before (solid red) and after (solid purple) reaction with propene. Dashed grey lines correspond to metallic Ru reference.

#	Catalyst/Substrate	CO (bar)	H₂ (bar)	T (°C)
1	$RuBr_3$ in Bu_4PBr (Ru:Br = 1:35)[a]	1	20	180
2		5	–	180
3		5	15	180
4	$RuBr_3$ in Bu_4PBr (Ru:Br = 1:170)[b]	–	–	180
5		–	15	180
6		–	15	220
7	$[RuBr_2(CO)_3]_2$ in Bu_4PBr (1:170)	–	–	180
8		–	20	220
9	$[RuCl_2(CO)_3]_2$ in Bu_4PBr (1:170)	–	–	180
10		–	20	220
11	$RuBr_3$ in Bu_4PBr + Formaldehyde[c]	–	–	180
12		–	15	220
13	$RuBr_3$ in Bu_4PBr (1:170) + IPA[d] in air	–	–	120
14	$RuBr_3$ in Bu_4PBr (1:170) + IPA[d]	–	30	200
15	+ additional Formaldehyde[c]	–	30	200
16	$[RuBr_2(CO)_3]_2$ in Bu_4PBr (1:170) + IPA[d]	–	30	200

Fig. 7 (a) XANES spectra of pure Ru-species (solid coloured lines) extracted by MCR-ALS plotted together with the reference spectra of $RuBr_3$, $[RuBr_2(CO)_3]_2$, and Ru foil (dashed red, green and blue lines respectively). (b) Concentration profiles of the three Ru-species extracted from MCR-ALS. (c) A list of experimental conditions applied during *in situ* XAS data collection. Conditions were varied within the described boundary conditions (see ESI,† "boundary conditions"): CO (0–5 bar), H₂ (0–30 bar) and temperature (180–220 °C). Dashed lines indicate when the sample was changed. [a]A high concentration of $RuBr_3$ was used, with 68 mg $RuBr_3$ in 2 g IL. [b]For all other entries, low concentrations of Ru were measured (13.6 mg in 2 g IL, similar to catalytic results presented in Table 1). [c]Formaldehyde (100 μL) was thermally decomposed to generate *in situ* CO gas. [d]Isopropanol (IPA, 250 μL) was added as propene precursor.

not active in carbonyl hydrogenation and can be responsible for alkene hydrogenation (Table 1; entry 1 and 8).

In situ evolution of Ru-species under reaction conditions

To prove the relevance of the Ru-species identified from *ex situ* data, an *in situ* experiment was performed utilizing a dedicated high-pressure reactor cell (see Fig. S1†). The data (Fig. S3†) were collected in fluorescence mode with high time resolution and have lower signal-to-noise ratio for quantitative EXAFS analysis than in measurements performed on *ex situ* samples. Implementation of PCA and MCR-ALS procedures to the whole experimental dataset revealed the existence of three different Ru-species (see Fig. S4†); their spectra and respective concentration profiles are shown in Fig. 7. The fact that only three components were identified also indicates that no other Ru bromide carbonyl complex besides $[RuBr_2(CO)_3]_2$ is present in the system. Indeed, a complex with different Br/CO coordination numbers would result in similar spectral features but shifted edge position due to changes in Ru oxidation state,[9] which would result in an additional component in PCA.

The first part of Fig. 7(a) shows the spectra of pure species extracted from the *in situ* collected data. The first species is obviously similar to the RuBr$_3$ reference and to RuBr$_x$ dissolved in Bu$_4$PBr (indicated in red). The second species presents a spectrum close to that of the $[RuBr_2(CO)_3]_2$ reference and represents the Ru carbonyl contribution (indicated in green). Finally, the third species shares common features with metallic ruthenium foil (indicated in blue). The evolution of these three species under various conditions is summarized in Fig. 7b. The applied steps and corresponding sets of conditions (1–16) along

the *x*-axis are summarized in Fig. 7c, in which each scan takes approximately 5–6 minutes.

Under 1 bar CO and 20 bar H$_2$, a considerable fraction of RuBr$_x$ still remains unchanged for the highly concentrated catalyst (1). The fraction of Ru bromide carbonyl increases either by removing H$_2$ and increasing CO pressure (2) or by reducing the Ru loading (3), *i.e.* increasing CO/Ru ratio. In absence of CO, under inert atmosphere (4), in H$_2$ (5) and with increased temperature (6), Ru is gradually converted towards RuBr$_x$ species. In agreement with *ex situ* results, isolated $[RuX_2(CO)_3]_2$ complexes (7–8 and 9–10, respectively) contain less Ru carbonyl contribution (indicated in green) compared to the *in situ* carbonylated species (*i.e.* in step 3). Like in the previous research,[6] formaldehyde can also be used as a CO source (11–12). In presence of IPA (as propene precursor) and H$_2$ gas, RuBr$_x$ species are reduced to small Ru clusters (14). As expected, the RuBr$_x$ can be converted back to a Ru carbonyl species by addition of a CO source (formaldehyde, 15), while the lost Ru (0) species cannot. The metallic Ru contribution remains constant in step 14 *vs.* 15 (indicated in blue). If $[RuBr_2(CO)_3]_2$ is used as a precursor, slight decarbonylation is observed over a large timeframe of *ca.* 2.5 h (16).

The origin of the selectivity towards ketone hydrogenation

Since both *in situ* and *ex situ* experiments have unambiguously proven that $[RuBr_2(CO)_3]_2$ is the main active species necessary for the C=O hydrogenation, a screening of possible intermediate states in the hydrogenation of acetone and propene was performed at DFT level of theory, based on the minimal energy of their relaxed structures. In addition, the transition states and
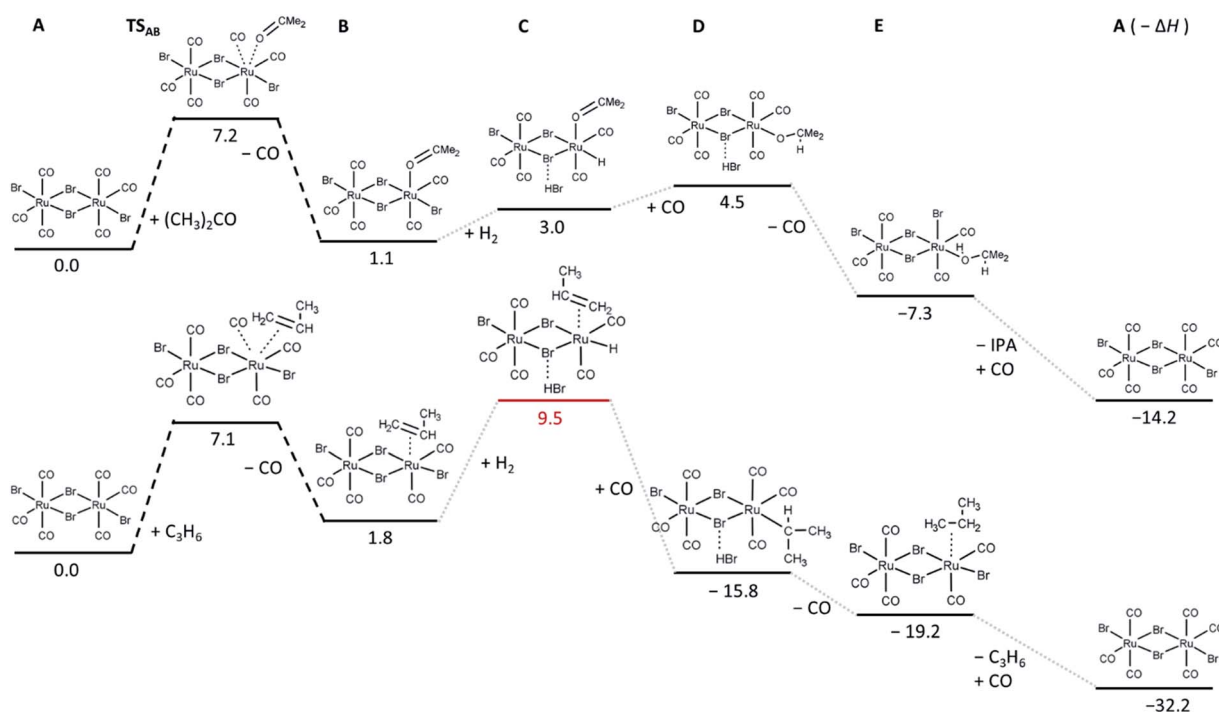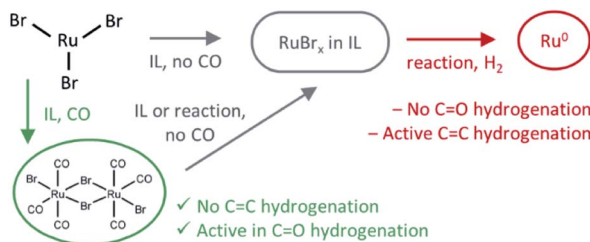

Fig. 8 Relative energies in kcal mol^{-1} of the most stable intermediates and first transition state determined for acetone (top) and propene (bottom) hydrogenation reactions. The corresponding relaxed structures and output files are attached in ESI.†

Scheme 2 Evolution of Ru-species depending on reaction conditions.

the height of the barriers for the adsorption of acetone and propene on the Ru complex were determined (Fig. 8).

In particular, the exchange of a CO ligand by acetone results in very small (in case of one-side reaction) or slightly negative (in case of both Ru-sites involved, shown in Fig. S6†) reaction enthalpies (Fig. 8), with an energy barrier of about 7 kcal mol^{-1}. Relatively small reaction enthalpies are also obtained for the next intermediate steps (dissociation of H$_2$ and carbonyl hydrogenation). For the hydrogenation of propene, the barrier for propene coordination instead of CO ligand is similar to that obtained for the acetone case, but it leads to the formation of an intermediate state with higher energy, indicating that in the competition, coordination of acetone is more favourable. The next step involving H$_2$ is significantly unfavourable compared to the acetone case, which might again explain the selectivity of the [RuBr$_2$(CO)$_3$]$_2$ system towards C=O hydrogenation over C=C hydrogenation. C=C hydrogenation over Ru^0 was not simulated, since olefin hydrogenation over active noble metal nanoparticles is well known.

Conclusions

Combining catalytic testing with in-depth characterization of the local structure of Ru-atoms by XANES and EXAFS, we have unambiguously shown the evolution of Ru-species and established important structure–activity and structure–selectivity relationships which were additionally supported by theoretical computations. The active [RuBr$_2$(CO)$_3$]$_2$ species are formed from RuBr$_3$ in Bu$_4$PBr in presence of CO gas during a pretreatment step, which is crucial to convert dissolved RuBr$_x$ into the active complex. These species selectively hydrogenate C=O bonds over C=C bonds due to favored coordination of ketones over alkenes on Ru sites and unfavorable intermediate states involving H$_2$ dissociation for the latter case, exemplified using acetone and propene as a substrate. Without a CO source, these species can disintegrate to RuBr$_x$ which under reaction conditions could be reduced to Ru^0 clusters responsible for unselective C=C hydrogenation. Disintegration to RuBr$_x$ occurs in the IL in absence of CO and when the pre-made catalysts are dissolved and CO is lost; this was the case for both [RuX$_2$(CO)$_3$]$_2$ (X = Br,Cl) complexes. If a Cl-containing precursor is used, a Cl$^-$–Br$^-$ exchange was identified in the Br-rich environment (IL) for all studied samples, resulting in the formation of the corresponding Br-containing complexes. These results give a complete understanding of the evolution of Ru species,

summarized in Scheme 2, applied for the homogeneous catalytic valorization of biobased (waste) polyols to olefins, indicating the undesired routes of its deactivation and possibilities for reactivation.

Data availability

The datasets supporting this article have been uploaded as part of the ESI material.†

Author contributions

K. J. performed the synthesis and catalytic testing. K. J., A. L. B., V. L. S. S., A. A. G., E. G. K. and O. A. U. measured XAS data. A. L. B. and E. G. K., performed XAS analysis and DFT calculations. K. J. and A. L. B. wrote the manuscript. A. V. S. and D. D. V. provided the funding, did the conceptualization and critical reading of the manuscript.

Conflicts of interest

There are no conflicts to declare.

Acknowledgements

Notes and references

1 P. A. Dub and J. C. Gordon, *Nat. Rev. Chem.*, 2018, **2**, 396–408.
2 D. Evans, J. A. Osborn, F. H. Jardine and G. Wilkinson, *Nature*, 1965, **208**, 1203–1204.

3 T. Ohkuma, H. Ooka, S. Hashiguchi, T. Ikariya and R. Noyori, *J. Am. Chem. Soc.*, 1995, **117**, 2675–2676.

4 R. Noyori and T. Ohkuma, *Angew. Chem., Int. Ed.*, 2001, **40**, 40–73.

5 G. Braca, A. M. Raspolli Galletti and G. Sbrana, *J. Organomet. Chem.*, 1991, **417**, 41–49.

6 M. Stalpaert, K. Janssens, C. Marquez, M. Henrion, A. L. Bugaev, A. V. Soldatov and D. E. De Vos, *ACS Catal.*, 2020, **10**, 9401–9409.

7 K. Janssens, M. Stalpaert, M. Henrion and D. E. De Vos, *Chem. Commun.*, 2021, **57**, 6324–6327.

8 B. F. G. Johnson, R. D. Johnston, P. L. Josty, J. Lewis and I. G. Williams, *Nature*, 1967, **213**, 901–902.

9 E. G. Kozyr, A. L. Bugaev, S. A. Guda, A. A. Guda, K. A. Lomachenko, K. Janssens, S. Smolders, D. De Vos and A. V. Soldatov, *J. Phys. Chem. C*, 2021, **125**, 27844–27852.

10 A. Martini, A. L. Bugaev, S. A. Guda, A. A. Guda, E. Priola, E. Borfecchia, S. Smolders, K. Janssens, D. De Vos and A. V. Soldatov, *J. Phys. Chem. A*, 2021, **125**, 7080–7091.

11 B. Ravel and M. Newville, *J. Synchrotron Radiat.*, 2005, **12**, 537–541.

12 S. I. Zabinsky, J. J. Rehr, A. Ankudinov, R. C. Albers and M. J. Eller, *Phys. Rev. B*, 1995, **52**, 2995–3009.

13 A. Martini, S. A. Guda, A. A. Guda, G. Smolentsev, A. Algasov, O. Usoltsev, M. A. Soldatov, A. Bugaev, Y. Rusalev, C. Lamberti and A. V. Soldatov, *Comput. Phys. Commun.*, 2020, **250**, 107064.

14 J. Jaumot, R. Gargallo, A. de Juan and R. Tauler, *Chemom. Intell. Lab. Syst.*, 2005, **76**, 101–110.

15 R. Tauler, *Chemom. Intell. Lab. Syst.*, 1995, **30**, 133–146.

16 J. Jaumot, A. de Juan and R. Tauler, *Chemom. Intell. Lab. Syst.*, 2015, **140**, 1–12.

17 G. te Velde, F. M. Bickelhaupt, E. J. Baerends, C. Fonseca Guerra, S. J. A. van Gisbergen, J. G. Snijders and T. Ziegler, *J. Comput. Chem.*, 2001, **22**, 931–967.

18 A. D. Becke, *Phys. Rev. A*, 1988, **38**, 3098–3100.

19 S. Grimme, J. Antony, S. Ehrlich and H. Krieg, *J. Chem. Phys.*, 2010, **132**, 154104.

20 C. Lee, W. Yang and R. G. Parr, *Phys. Rev. B*, 1988, **37**, 785–789.

21 E. van Lenthe and E. J. Baerends, *J. Comput. Chem.*, 2003, **24**, 1142–1156.

22 E. van Lenthe, A. Ehlers and E.-J. Baerends, *J. Chem. Phys.*, 1999, **110**, 8943–8953.

23 B. F. G. Johnson, R. D. Johnston and J. Lewis, *J. Chem. Soc. A*, 1969, 792–797.